9-1-2008

Two-Layer Hall-Effect Model with Arbitrary Surface-Donor Profiles: Application to ZnO

David C. Look
Wright State University - Main Campus, david.look@wright.edu

Two-layer Hall-effect model with arbitrary surface-donor profiles: application to ZnO

D. C. Look[1,2,a)]
[1]*Semiconductor Research Center, Wright State University, Dayton, Ohio 45435, USA*
[2]*Materials and Manufacturing Directorate, Air Force Research Laboratory, Wright-Patterson Air Force Base, Ohio 45433, USA*

(Received 30 May 2008; accepted 6 August 2008; published online 29 September 2008)

A complete two-layer Hall-effect model, allowing arbitrary donor and acceptor profiles, is presented and applied to the problem of conductive surface layers in ZnO. Temperature-dependent mobility and carrier concentration data in the temperature range of 20–320 K are fitted with an efficient algorithm easily implemented in commercial mathematics programs such as MATHCAD. The model is applied to two ZnO samples, grown by the melt (MLT) and hydrothermal (HYD) processes, respectively. Under the assumption of a "square" surface-donor profile, the fitted surface-layer thicknesses are 48 and 2.5 nm, respectively, for the MLT and HYD samples. The surface-donor concentrations are 7.6×10^{17} and 8.3×10^{18} cm^{-3}, and the *integrated* surface-donor concentrations are 2.1×10^{12} and 3.6×10^{12} cm^{-2}. For an assumed Gaussian $[N_{Ds}(0)\exp(-z^2/d_s^2)]$ donor profile, the fitted values of d_s are nearly the same as those for the square profile. The values of $N_{D,s}(0)$ are about 50% larger and the integrated donor-concentration values are about 15% larger, for both samples. As a surface-analysis tool, the Hall effect is extremely sensitive and applicable over a wide range of surface-layer conditions. © *2008 American Institute of Physics*. [DOI: 10.1063/1.2986143]

I. INTRODUCTION

The wide-band gap semiconductor ZnO is presently being evaluated for applications such as UV emitters and detectors, transparent transistors, gas sensors, and field emitters.[1–4] For these applications, and moreover, for virtually all devices formed from nanostructures, surface properties are very important. Although many techniques, such as Auger electron spectroscopy, secondary-ion mass spectroscopy (SIMS), and x-ray photoelectron spectroscopy, are useful for characterizing surfaces, none of them can directly identify donors and acceptors. This lack of donor/acceptor information from standard surface-analysis techniques has recently attained increased importance because we and others have found that most ZnO surfaces are *n*-type and highly conductive, implying high concentrations of donors.[5–11] Fortunately, we have also found that low-temperature Hall-effect measurements can be used to effectively characterize the surface conductivity and in fact quantitatively deduce the donor concentration in the surface region.[6,10,12] However, the actual identities of these surface donors must be determined by correlation with analytical techniques, such as SIMS. In one recent case we have accomplished such a correlation by showing that the conductive surface layer in that case was due to group-III donors (Al, Ga, and In) that had diffused into the surface region from the bulk during an anneal.[12] However, our Hall-effect fitting routine at that time was limited to analysis of only a "square" surface-donor profile, i.e., a constant N_{Ds} from the surface to a thickness d_s, and a vanishing N_{Ds} beyond that point. The SIMS measurements, on the other hand, showed a sharply sloped profile of the group-III atoms resembling an exponential shape. Since the $1/e$ amplitude of the SIMS profile was close to the value of d_s determined from the Hall measurements and since the integrated SIMS profile was about equal to the sheet donor concentration $N_{Ds}\times d_s$, it was clear in that case that the donors were indeed composed of group-III atoms that had diffused into the surface region. However, it was also evident that the Hall-effect model would have to be extended to allow arbitrarily shaped donor profiles, which is one of the purposes of the present paper. We also present a new, simple, efficient multiparameter fitting routine, encompassing both bulk and surface conductions, and apply it to commercially available ZnO samples grown by the hydrothermal (HYD) and melt (MLT) methods. A convenient implementation of the fitting routine is available from the author.

II. HALL-EFFECT THEORY

Consider a thin plate that is inhomogeneous but only in the dimension z perpendicular to the plate. Then, the theoretical Hall mobility and carrier concentration in such a sample can be written as[13,14]

$$\mu_{H,\mathrm{theo}}(T)=\frac{\int_0^d \mu_{\mathrm{Cond}}(T,z)\mu_H(T,z)n(T,z)dz}{\int_0^d \mu_{\mathrm{Cond}}(T,z)n(T,z)dz}, \tag{1}$$

$$n_{\mathrm{theo}}(T)=\frac{1}{d}\frac{\left[\int_0^d \mu_{\mathrm{Cond}}(T,z)n(T,z)dz\right]^2}{\int_0^d \mu_{\mathrm{Cond}}(T,z)\mu_H(T,z)n(T,z)dz}, \tag{2}$$

where T is temperature, d is the total sample thickness (typically 0.5 mm for the samples of this study), μ_{Cond} is the

a)Electronic mail: David.Look@WPAFB.AF.MIL.

conductivity mobility, and μ_H the Hall mobility, both of which will be defined later. In as-grown or annealed bulk ZnO samples, it is typical to find a thin, highly conductive layer of approximate thickness d_s, where d_s can range from 1–50 nm for samples of the type studied here.[10] The electrons in this surface layer are usually degenerate, i.e., their concentration n_s is constant with temperature. Most of the rest of the sample, i.e., $d_s < z \leq d$, contains nondegenerate electrons with uniform electrical properties, and we call this region the "bulk" part. Thus, for practical purposes we can simplify Eqs. (1) and (2) as follows:

$$\mu_{H,\mathrm{theo}}(T) = \frac{\int_0^{d_s} \mu_{\mathrm{Cond},s}(T,z)^2 n_s(T,z)dz + (d-d_s)\mu_{\mathrm{Cond},b}(T)\mu_{H,b}(T)n_b(T)}{\int_0^{d_s} \mu_{\mathrm{Cond},s}(T,z) n_s(T,z)dz + (d-d_s)\mu_{\mathrm{Cond},b}(T)n_b(T)}, \tag{3}$$

$$n_{\mathrm{theo}}(T) = \frac{1}{d}\frac{\left[\int_0^{d_s} \mu_{\mathrm{Cond},s}(T,z) n_s(T,z)dz + (d-d_s)\mu_{\mathrm{Cond},b}(T)n_b(T)\right]^2}{\int_0^{d_s} \mu_{\mathrm{Cond},s}(T,z)^2 n_s(T,z)dz + (d-d_s)\mu_{\mathrm{Cond},b}(T)\mu_{H,b}(T)n_b(T)}, \tag{4}$$

where $\mu_{\mathrm{Cond},b}(T)$, $\mu_{H,b}(T)$, and $n_b(T)$ represent the uniform, bulk region, $d_s < z \leq d$. It is also important to note that we have explicitly set $\mu_{H,s}(T,z) = \mu_{\mathrm{Cond},s}(T,z)$ for the electrons in the surface region because, as is well known, the Hall mobility is equal to the conductivity mobility for degenerate electrons. Finally, for a square profile, which does not require integration and is often a fast, useful approximation, we have

$$\mu_{H,\mathrm{theo}}(T) = \frac{d_s\mu_{\mathrm{Cond},s}(T)^2 n_s(T) + (d-d_s)\mu_{\mathrm{Cond},b}(T)\mu_{H,b}(T)n_b(T)}{d_s\mu_{\mathrm{Cond},s}(T) n_s(T) + (d-d_s)\mu_{\mathrm{Cond},b}(T)n_b(T)}, \tag{5}$$

$$n_{\mathrm{theo}}(T) = \frac{1}{d}\frac{[d_s\mu_{\mathrm{Cond},s}(T) n_s(T) + (d-d_s)\mu_{\mathrm{Cond},b}(T)n_b(T)]^2}{d_s\mu_{\mathrm{Cond},s}(T)^2 n_s(T) + (d-d_s)\mu_{\mathrm{Cond},b}(T)\mu_{H,b}(T)n_b(T)}. \tag{6}$$

We first consider the nondegenerate carrier concentration $n_b(T)$ in the uniform, bulk part of the sample. For a single donor of concentration $N_{D,b}$, with activation energy $E_{D,b}$, we can write[14]

$$n_b(T) = \frac{1}{2}[\phi(T) + N_{A,b}] \times \left\{\left\{1 + \frac{4\phi(T)(N_{D,b} - N_{A,b})}{[\phi(T) + N_{A,b}]^2}\right\}^{1/2} - 1\right\}, \tag{7}$$

where $N_{A,b}$ is the concentration of all acceptors below the Fermi level (basically, all acceptors in the sample if the Fermi level is near the conduction band edge), and $\phi(T) = [2(2\pi m^* kT)^{3/2}/h^3](g_0/g_1)\exp(-E_{D,b}/kT) = 7.94 \times 10^{14}\ T^{3/2}(g_0/g_1)\exp(-E_{D,b}/kT)$, in units of cm^{-3}, for ZnO ($m^* = 0.3m_0$). Here (g_0/g_1) is a degeneracy factor, typically equal to $\frac{1}{2}$ for a simple donor. The carrier concentration $n_s(T,z)$ in the surface region is much simpler: $n_s(T,z) = [N_{D,s}(0) - N_{A,s}(0)]P(z,d_s)$, where $P(z,d_s)$ is the profile of the surface donors and acceptors. In this work, we will assume that $N_{D,s}(0) \gg N_{A,s}(0)$, and further limit $P(z,d_s)$ to an exponential form $N_{D,s}(0)$ $[\exp(-z/d_s)]$, Gaussian form $N_{D,s}(0)$ $[\exp(-z^2/d_s^2)]$, or square form $N_{D,s}(0)\Phi(d_s - z)$, where $\Phi(d_s - z)$ is the Heaviside function, equal to one for $z \leq d_s$ and zero otherwise. Other forms of $P(z,d_s)$ can also easily be accommodated because Eqs. (3) and (4) use numerical integration over depth z.

For the mobility, we assume a nondegenerate form for both the surface and bulk regions because, unlike the surface carrier concentration, the surface mobility is dependent on temperature for nearly all the ZnO samples that we have measured. In the relaxation-time (τ) approximation, the mobility can be written in terms of $\langle \tau(x,T,z)^n \rangle$, where the brackets $\langle\rangle$ denote an average over normalized energy x ($x = E/kT$). For nondegenerate electrons, the energy average is determined from[14]

$$\langle \tau(T,z)^n \rangle = \frac{4}{3\pi^{1/2}} \int_0^{20} x^{3/2} \tau(x,T,z)^n e^{-x} dx, \tag{8}$$

where n is an integer and where the upper limit in the integral ($x = 20$) is large enough to provide good accuracy. In terms of Eq. (8), the conductivity mobility is defined as $\mu_{\mathrm{Cond}}(T,z) = e\langle \tau(T,z) \rangle / m^*$, where m^* is the effective mass, and the Hall mobility, $\mu_H(T,z) = e\langle \tau(T,z)^2 \rangle / m^* \langle \tau(T,z) \rangle$. The total relaxation time $\tau(T,z)$ has contributions from a number of different scattering mechanisms and can be found by adding their relaxation *rates* (inverse relaxation times):

$$\tau(x,T,z)^{-1} = \tau_{po}(x,T)^{-1} + \tau_{ac}(x,T)^{-1} + \tau_{pe}(x,T)^{-1} + \tau_{ii}(x,T,z)^{-1} + \tau_{sc}(x,T)^{-1} + \tau_{\mathrm{dis}}(x,T)^{-1}. \tag{9}$$

The scattering in each case results from variations in potential due to departures from perfect crystal symmetry. For τ_{po}, optical-mode lattice vibrations produce changes in the

atomic polarization in ionic crystals. For τ_{ac} and τ_{pe}, acoustic-mode lattice vibrations produce changes in lattice position or polarization, respectively. For τ_{ii} and $\tau_{\rm dis}$, ionized impurities and point defects or charged dislocations, respectively, produce coulomb potentials. Finally, for τ_{sc}, several types of space-charge regions act as impenetrable barriers. The scattering events represented by τ_{ac}, τ_{pe}, τ_{ii}, $\tau_{\rm dis}$, and τ_{sc} involve only small changes of energy, and thus can be accurately modeled by the relaxation-time analysis presented here. However, polar-optical scattering (τ_{po}) is an exception because here each scattering event exchanges an optical phonon of energy $\hbar\omega_{po}=72$ meV. Thus, strictly speaking, we cannot define a relaxation time for polar-optical scattering and our analysis is not valid; however, we have found an approximate formula for $\tau_{po}(x,T)$ that reproduces the more accurate result (e.g., that given by an iterative solution of the Boltzmann equation) reasonably well. Another justification for use of this approximate formula is that none of the important fitting parameters resulting from this analysis ($N_{D,s}$, d_s, $N_{A,b}$, $N_{D,b}$, and $E_{D,b}$) are sensitive to the strength of the polar-optical scattering. Thus, we suggest the following empirical form for $\tau_{po}(x,T)$:

$$\tau_{po}(x,T)=\frac{2^{3/2}\pi\hbar^2}{e^2kT_{po}m^{*1/2}(\varepsilon_\infty^{-1}-\varepsilon_0^{-1})}(e^{T_{po}/T}-1)\times[0.5446(xkT)^{1/2}+0.5888(kT_{po})^{1/2}-0.1683(kT_{po})^{-1/2}(xkT)], \tag{10}$$

where MKS units are used here and below unless otherwise specified, and the term preceeding the $[\exp(T_{po}/T)-1]$ term is 3.873×10^{-5} for ZnO ($T_{po}=\hbar\omega_{po}/k=837$ K, $\varepsilon_0=8.12\varepsilon_{\rm vac}$, and $\varepsilon_\infty=3.72\varepsilon_{\rm vac}$). The other relaxation times can be written as follows:[14–16]

$$\tau_{ac}(x,T)=\frac{\pi\hbar^4\rho s^2}{2^{1/2}m^{*3/2}ke^2E_1^2}\frac{(xkT)^{-1/2}}{T}=4.937\times10^{-21}\frac{(xkT)^{-1/2}}{T}, \tag{11}$$

where $\rho=5.675\times10^3$ kg/m^3, $s=6.006\times10^3$ m/s, and E1 is the acoustic deformation potential in electron volts, taken as 15 eV for ZnO,

$$\tau_{pe}(x,T)=\frac{2^{3/2}\pi\hbar^2\varepsilon_0}{e^2m^{*1/2}kP_{pe}^2}\frac{(xkT)^{1/2}}{T}=0.8696\frac{(xkT)^{1/2}}{T}, \tag{12}$$

where P_{pe} is the unitless piezoelectric coupling coefficient, taken to be 0.21 for ZnO,

$$\tau_{sc}(x,T,R_{sc})=\frac{m^{*1/2}(10^{-9}R_{sc})}{2^{1/2}}(xkT)^{-1/2}=3.696\times10^{-25}R_{sc}(nm)(xkT)^{-1/2}, \tag{13}$$

where R_{sc} is a fitting parameter in nanometer. Finally, for ionized-impurity scattering in the bulk region (*nondegenerate* electrons),

$$\tau_{ii,b}(x,T)=\frac{2^{1/2}16\pi\varepsilon_0^2m^{*1/2}}{e^4}\times\left[\frac{(xkT)^{3/2}}{\left(\{[2N_{A,b}(T)+n_b(T)]10^6\}\times\left\{\ln[1+y_b(x,T)]-\frac{y_b(x,T)}{1+y_b(x,T)}\right\}\right)}\right], \tag{14}$$

where the first term is 2.915×10^{41} for ZnO, and the units of $N_{A,b}(T)$ and $n_b(T)$ are cm^{-3}; also,

$$y_b(x,T)=\frac{8\varepsilon_0m^*k}{\hbar^2e^2}\frac{(xkT)T}{n_b(T)}=7.601\times10^{42}\frac{(xkT)T}{n_b(T)10^6}, \tag{15}$$

where again, $n_b(T)$ is in units of cm^3. In the surface region, we continue to use the nondegenerate formula for mobility, since the mobility is typically temperature-dependent, but a degenerate form of the screening function $y(z)$, since the carrier concentration is usually temperature-independent:

$$\tau_{ii,s}(x,T,z)=\frac{2^{1/2}16\pi\varepsilon_0^2m^{*1/2}}{e^4}\times\left[\frac{(xkT)^{3/2}}{\left(\{2[N_{A,s}(0)P(z,d_s)+n_s(z)]10^6\}\times\left[\ln(1+y_s(z))-\frac{y_s(z)}{1+y_s(z)}\right]\right)}\right], \tag{16}$$

where, as mentioned above, the first term is 2.915×10^{41}, and $N_{D,s}(0)$ and $n_s(z)$ have units of cm^{-3}. The degenerate form of $y_s(z)$ is

$$y_s(z)=\frac{3^{1/3}4\pi^{8/3}\varepsilon_0\hbar^2}{e^2m^*}\{[N_{D,s}(0)-N_{A,s}(0)]P(z,d_s)10^6\}^{1/3}=1.392\times10^{-8}\{[N_{D,s}(0)-N_{A,s}(0)]P(z,d_s)10^6\}^{1/3}. \tag{17}$$

For completeness, we also give the nondegenerate formula for threading-edge dislocation scattering in the bulk region,[17]

$$\tau_{{\rm dis},b}(x,T)=\frac{\hbar^3\varepsilon_0^2c_{\rm latt}^2}{N_{\rm dis}10^4m^*e^4}\frac{\left\{1+\frac{8m^*\lambda_b(T)^2xkT}{\hbar^2}\right\}^{3/2}}{\lambda_b(T)^4}=\frac{9.1273\times10^{-40}}{N_{\rm dis}}\frac{\{1+1.9658\times10^{38}\lambda_b(T)^2xkT\}^{3/2}}{\lambda_b(T)^4}, \tag{18}$$

where $N_{\rm dis}$ is the dislocation density in units of cm^{-2} and it is assumed that there is one electronic charge per c-lattice distance, where $c_{\rm latt}=5.207\times10^{-10}$ m. The screening parameter $\lambda_b(T)$ is given by

$$\lambda_b(T)=\left\{\frac{\varepsilon_0kT}{e^2n_b(T)10^6}\right\}^{1/2}=0.1966\left\{\frac{T}{n_b(T)}\right\}^{1/2}, \tag{19}$$

where $n_b(T)$ is in units of cm^{-3}, and $\lambda_b(T)$, in meters. For the single crystals used in the study, the dislocation densities are on the order of 10^5 cm^{-2} or less and thus will not affect the mobility significantly. However, for lattice-mismatched

growth, dislocation scattering may have to be included in the analysis.

Equations (10)–(17) are inserted into Eq. (9) to give the overall relaxation time $\tau(x,T,z)$. Then τ is averaged over normalized energy x in Eq. (8), and finally the theoretical values of mobility $\mu_{H,\text{theo}}(T)$ and carrier concentration $n_{\text{theo}}(T)$ are calculated for an arbitrary profile in Eqs. (3) and (4), or for a simple square profile in Eqs. (5) and (6). The goal of our study is to find a set of six fitting parameters, $N_{Ds}(0)$, d_s, N_{Ab}, N_{Db}, E_{Db}, and R_{sc}, which best matches the calculated $\mu_{H,\text{theo}}(T)$ and $n_{\text{theo}}(T)$ curves with the experimental curves, $\mu_{H,\text{expt}}(T)$ and $n_{\text{expt}}(T)$, respectively. The normal methodology for finding such a set of multiple fitting parameters is to employ some type of general, least-squares fitting routine; however, when implemented on typical personal computers, such multiple-parameter routines are often quite slow. We have developed an alternative scheme that breaks the six-parameter fit into six, single-parameter fits. In this scheme, we fit either $\mu_{H,\text{theo}}(T_i)$ to $\mu_{H,\text{expt}}(T_i)$ or $n_{\text{theo}}(T_i)$ to $n_{\text{expt}}(T_i)$ at up to six different temperature points T_i. One convenient implementation of this model is to fit *both* $\mu_{H,\text{theo}}(T_i)$ and $n_{\text{theo}}(T_i)$ at only three well-chosen temperature points T_1, T_2, and T_3, giving six independent equations to fit the six parameters. Here, T_1 is usually the lowest experimental temperature, T_3, the highest, and T_2, an intermediate point near the mobility maximum. The fitting sequence is important. We begin in step 1 by recognizing that surface conduction is most dominant in the lowest temperature region and that therefore $\mu(T_1)$ will be mainly determined by $N_{Ds}(0)$. Then, in step 2, $n(T_1)$ will depend almost entirely on d_s along with $N_{Ds}(0)$, which has already been determined in step 1. In step 3, $\mu(T_2)$ is found by varying $N_{A,b}$, which is by far the most important determinant of maximum mobility at least among the four remaining parameters. Then, in step 4, a good approximation to $n(T_3)$ can be found by varying $N_{D,b}$ because, if T_3 is a high temperature, then $n_b \sim N_{D,b} - N_{A,b}$ and we have just found $N_{A,b}$ in the previous step. In step 5, we vary $E_{D,b}$ to fit $n(T_2)$ because, as T increases, the rapidity with which the bulk carrier concentration n_b becomes more important than the surface-electron concentration n_s depends predominantly on $E_{D,b}$. Finally, in step 6, we vary R_{sc} to fit $\mu(T_3)$ because, if ionized-impurity scattering is relatively weak, then the only additional nonlattice-scattering mechanism in our model is space-charge scattering. Indeed, even though we may not always fully understand the origins of the space-charge regions, still we have often found that the inclusion of space-charge scattering is necessary to achieve good mobility fits over the whole temperature range, especially at high temperatures.

In our laboratory, we accomplish each of the six independent fits by means of the "root" function in the commercial mathematical program MATHCAD;[18] however, the ideas presented here should be easily transferable to other mathematical environments. A detailed description of the fitting program implemented in MATHCAD is presented in Appendix. Also, an actual MATHCAD file that performs the calculations for an arbitrary number of iterations is available by electronic mail from the author.[19]

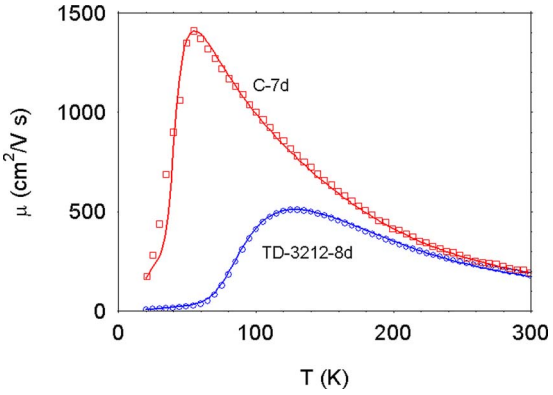

FIG. 1. (Color online) Temperature-dependent mobility data for ZnO samples C-7d and TD-3212–8d. The solid lines are fits determined from the Gaussian parameters in Table I.

III. EXPERIMENTAL CONSIDERATIONS

The two ZnO samples used in the present study were $5 \times 5 \times 0.5$ mm^3, [0001]-oriented plates cut from 10×10 mm^2 plates supplied by the respective manufacturers. One sample, C-7d, was grown by Cermet, Inc.[20] using a pressurized-melt method and its electrical properties are in many ways typical of material grown by either the MLT or vapor-phase (VP) techniques. The other sample, TD-3212–8d, was grown by Tokyo Denpa[21] using a HYD method. Its electrical properties were much different, as is the case for all HYD samples that we have studied. For example, HYD samples typically have higher acceptor concentrations, lower donor concentrations, and much closer compensation than MLT or VP samples.[22] These properties can be changed by annealing in various ambients[22] but such modifications will not be discussed here.

Temperature-dependent (20–320 K) Hall-effect (T-Hall) measurements were performed with a LakeShore 7507 system. Ohmic contacts were formed by soldering In dots on the corners of each sample. As we have shown previously, the low-temperature data are usually dominated by near-surface electrons because the bulk electrons are frozen out onto their parent donors. The room-temperature properties, on the other hand, are mainly determined by the bulk electrons because of their much higher mobilities.[6,10,12,22]

The T-Hall data are presented in Fig. 1 (mobility) and Fig. 2 (carrier concentration). The solid lines in these figures are solutions of Eqs. (3) and (4), using the "Gaussian" parameters in columns 4 and 7 of Table I for samples TD-3212–8d and C-7d, respectively. However, the square parameters in columns 2 and 5, or "exponential" parameters in columns 3 and 6, also will produce equally good fits of the data. The Gaussian and square profiles derived from the associated $N_{D,s}(0)$ and d_s parameters in Table I are shown in Fig. 3: $N_{D,s}(z) = N_{D,s}(0)\exp(-z^2/d_s^2)$ for the Gaussian profiles, and $N_{D,s}(z) = N_{D,s}(0)$, $z \le d_s$, and $N_{D,s}(z) = 0$, $z > d_s$, for the square profiles. The exponential profiles are not shown in Fig. 3 to avoid clutter.

IV. DISCUSSION

We have no direct analytical data on either of the two ZnO samples used in this study. However, we do have SIMS

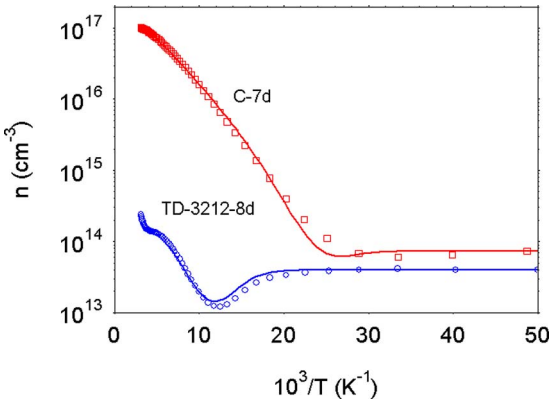

FIG. 2. (Color online) Temperature-dependent carrier concentration data for ZnO samples C-7d and TD-3212–8d. The solid lines are fits determined from the Gaussian parameters in Table I.

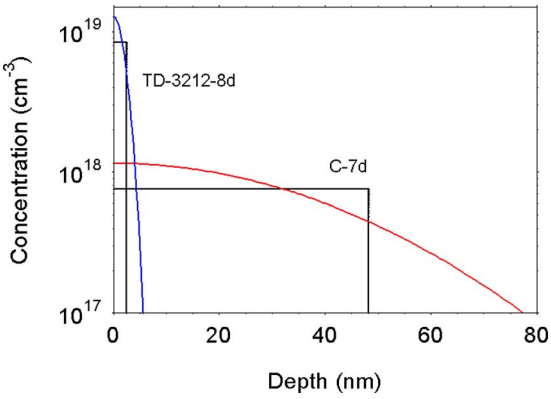

FIG. 3. (Color online) The square and Gaussian donor-concentration profiles based on the fitted values of $N_{D,s}(0)$, and d_s found in Table I: columns 2 and 4, for sample TD-3212–8d, and columns 5 and 7, for sample C-7d, respectively.

data on another sample, TD-R59–2b, which was grown under the same conditions as those of TD-3212–8d.[12] The SIMS data on TD-R59–2b can be briefly summarized as follows: (1) adding the group-III donor concentrations, [group −III]=[Al]+[Ga]+[In], gives a flat concentration of about 1×10^{17} cm^{-3} in the bulk ($z>100$ nm), and a roughly exponential profile with $N_{D,s}(0)=1.5\times10^{20}$ cm^{-3} and $d_s=3.7$ nm near the surface. (2) The Li concentration [Li] is also about 1×10^{17} cm^{-3} in the bulk but rises only to about 1×10^{18} cm^{-3} at the surface. If indeed, TD-3212–8d is much like TD-R59–2b, and if the group-III elements are the dominant donors and Li the dominant acceptor, then the close compensation in the bulk (i.e., $N_{A,b}\approx N_{D,b}$) and the donor dominance near the surface [i.e., $N_{A,s}(0)\ll N_{D,s}(0)$] are both explained.

A detailed discussion of the various bulk and surface properties is beyond the scope of this paper, and will be presented independently. However, we can at least compare the general shapes and magnitudes of the SIMS and Hall-effect profiles. Since the group-III SIMS profile of sample TD-R59–2b is roughly exponential, we choose for comparison the exponential Hall-effect profile of TD-3212–8d, represented by the values of $N_{D,s}(0)$ and d_s in column 3 of Table I. The Hall-derived value $N_{D,s}(0)=1.5\times10^{19}$ cm^{-3} is about a factor of ten lower than the group-III concentration at the surface but the Hall value of $d_s=2.6$ nm is reasonably close to that of the group-III elements, which is encouraging. There are at least three possible reasons for the $N_{D,s}(0)$ discrepancy: (1) the SIMS and Hall-effect samples are different and really cannot be compared, (2) a large fraction of the group-III elements are not active donors, or (3) the SIMS profile near the surface is artificially enhanced, which is often found to be the case. With regard to reason 2, it is interesting that the SIMS values of the group-III elements are about a factor of ten higher than the Hall-effect fitted values of N_D in *both* the surface region ($N_{D,s}$) and the bulk ($N_{D,b}$). However, further understanding of these issues will require more detailed analysis.

One conclusion from the present work is that, at least for these samples, the Hall-effect analysis alone is not sufficient to predict the profile of the surface donors, i.e., whether square, exponential, or Gaussian, or something else. Thus, we require further, independent data, such as that produced by SIMS, in order to determine the exact shape of the profile. However, one interesting observation is that if we analyze the Hall-effect data under the assumption of a square profile, then it turns out that we can immediately determine the "equivalent" exponential and Gaussian profiles with a fair degree of accuracy. That is, note from Table I that $N_{D,s}(0)_{\rm exp}/N_{D,s}(0)_{\rm sq}\approx1.8$ and $N_{D,s}(0)_{\rm Gauss}/N_{D,s}(0)_{\rm sq}\approx1.5$ for both samples TD-3212–8d and C-7d. Furthermore, $d_{s,\rm exp}/d_{s,\rm sq}\approx1.02$ and $d_{s,\rm Gauss}/d_{s,\rm sq}\approx1.02$ for both samples. This observation shows that most of the calculations can initially be carried out for a square profile, and thus Eqs. (5) and (6) can be employed rather than Eqs. (3) and (4). The

TABLE I. Fitted parameters, after five iterations, for as-grown ZnO samples TD-3212–8d and C-7d under assumptions of square, exponential, and Gaussian surface-donor profiles. Units: $N_{D,s}(0)$, $N_{A,b}$, and $N_{D,b}$, in 10^{16} cm^{-3}; d_s and R_{sc}, in nanometer; and $E_{D,b}$, in meV

Sample	TD-3212–8d			C-7d		
Profile	**square**	**exponential**	**Gaussian**	**square**	**exponential**	**Gaussian**
Parameter						
$N_{D,s}(0)$	835	1490	1280	75.8	135	115
d_s	2.52	2.56	2.57	48.2	49.3	49.5
$N_{A,b}$	1.342	1.344	1.344	0.261	0.260	0.260
$N_{D,b}$	1.355	1.357	1.357	12.9	12.9	12.9
$E_{D,b}$	50.0	49.8	49.7	41.7	41.7	41.7
R_{sc}	92.3	97.4	98.6	194	194	194

time savings in this case is considerable, about a factor of five, and thus, e.g., more iterations of Eqs. (A1)–(A6) can be run, leading to greater accuracy.

V. SUMMARY

In conclusion, we have presented a complete, physics-based model for analysis of temperature-dependent Hall-effect data on samples with both bulk and surface conductances. The model requires six fitting parameters: four characterizing the bulk, and two characterizing the surface. An efficient curve-fitting algorithm is developed, based on single-parameter fits of either mobility *or* carrier concentration at six given temperatures rather than on simultaneous six-parameter fits of both mobility and carrier concentration fits at all temperatures. Excellent fits of mobility and carrier concentration are obtained for two ZnO samples, grown by the MLT and HYD methods, respectively, and having very different electrical characteristics both in the bulk and the surface. In comparison to the MLT sample, the HYD sample has a much lower bulk donor concentration, a much higher bulk acceptor concentration, a much higher surface-donor concentration, and a much lower surface-layer thickness. Such differences, which are typical of HYD vs MLT (or VP) ZnO samples, are conveniently studied with the model presented here.

ACKNOWLEDGMENTS

We wish to thank T.A. Cooper for the Hall-effect measurements, L. Callahan for sample preparation, and B. Claflin for helpful discussions. Support is gratefully acknowledged from the following sources: AFOSR Grant No. FA9550-07-1-0013 (K. Reinhardt), NSF Grant No. DMR0513968 (L. Hess), DOE Grant No. DE-FG02-07ER46389 (R. Kortan), ARO Grant No. W911NF-07-D-0001/Task07275 (M. Gerhold), and AFRL Contract No. FA8650-06-D-5401 (S. Shell and D. Silversmith).

APPENDIX: IMPLEMENTATION OF DATA FITTING IN MATHCAD

Here we show how the data fitting can be accomplished by means of the root function in the commercial mathematical program MATHCAD.[18] To use the root function in MATHCAD, guesses of each of the six fitting parameters are first required; we designate this set of six parameters as set_0. As each root function is solved, the newly fitted parameter replaces the guessed value of that parameter in all of the succeeding root calculations; thus, following completion of the sixth root function, a new set of parameters, set_1, has been established. If desired, set_1 can then be used as a "guess" set to begin a new iteration of the six root equations, producing set_2. In general, by set_5, all parameters will have converged to within 0.1% of their final values. However, further iterations can be used if one or more of the parameters is still changing significantly, say, due to an initial poor guess. With regard to speed, each set can be calculated in 10–15 s on a typical desktop computer if Eqs. (3) and (4) are employed. However, for square profiles, which can be fitted with Eqs. (5) and (6), only 2–3 s per set are required.

The root function in MATHCAD is implemented as follows: suppose we have a function $f(\text{Par},x)$ in which Par is an adjustable parameter and we want to find the value of Par that produces $f(\text{Par},x_1)=B$ or $f(\text{Par},x_1)-B=0$ at some point x_1. Par is calculated by using the format: "Par $=\text{root}[f(\text{Par},x_1)-B,\text{Par}]$." We should also note as a practical matter that if B is a large number written in scientific notation as $B_0\times 10^n$, then the MATHCAD algorithm works more efficiently by writing the equivalent equation: "Par $=\text{root}[f(\text{Par},x_1)10^{-n}-B_0,\text{Par}]$." Finally, as stated above, the algorithm requires an initial guess of Par.

In our case, we have found that the following guess set works well for the two, very different samples studied in this work and is useful for many types of bulk ZnO: $N_{D,s}(0)=1\times 10^{18}$ cm^{-3}, $d_s=n_{\text{expt}}(T_1)\times d/N_{D,s}(0)$, $N_{A,b}=(0.1-2.0)\times 10^{16}$ cm^{-3}, $N_{D,b}=[N_{A,b}+n_{\text{expt}}(T_3)]$cm^{-3}, $E_{D,b}=0.05$ eV, and $R_{sc}=100$ nm. Of the six parameters, only $N_{A,b}$ seems to require a fairly good guess either to achieve an *initial* successful convergence of its particular root equation (step 3, Eq. (A3), Appendix) or to facilitate final convergence of all of the six root equations after only a few iterations. As an example, for sample C-7d (cf. Table I), a starting choice $N_{A,b}\geq 0.4\times 10^{16}$ cm^{-3} causes step 3 [Eq. (A3)] to "blow up" without finding any solution at all. However, any starting choice of $N_{A,b}<0.4\times 10^{16}$ cm^{-3} works very well and results in all six parameters converging to their final values (cf. Table I) in only three iterations (set_3). For sample TD-3212–8d, it turns out that the best starting range of $N_{A,b}$ is $1.3-1.40\times 10^{16}$ cm^{-3}, and this fact can be quickly determined by varying the starting values of $N_{A,b}$ from, say, $1.0-2.0\times 10^{16}$ cm^{-3} and observing the plots of mobility in each case after one iteration, which takes only about 10 s. It is found that the mobility fits turn out to be poor unless $1.3\times 10^{16}<N_{A,b}<1.5\times 10^{16}$ cm^{-3}, so this defines a good starting range for $N_{A,b}$. In short, it is useful to try several values of $N_{A,b}$ and compare the final results, especially since the calculations are fast anyway. When the final parameter set, say set_3, has been achieved, it is a good idea to compare $\mu_{H,\text{theo}}(T)$ with $\mu_{H,\text{expt}}(T)$ and $n_{\text{theo}}(T)$ with $n_{\text{expt}}(T)$ over the whole temperature range. This can be done with plots or calculations of the sums of squares of the differences, or both. If the fits are unsatisfactory for any initial choice of $N_{A,b}$, then a different choice of T_2 may yield better results.

For convenient implementation into MATHCAD, we give the actual working equations:

$$N_{D,s}(0)=\text{root}[\mu_{H,\text{theo}}(T_1)-\mu_{H,\text{expt}}(T_1),N_{D,s}(0)]$$
$$=\text{root}[\mu_{H,\text{theo}}(20.0)-7.01,N_{D,s}(0)], \quad \text{(A1)}$$

$$d_s=\text{root}[n_{\text{theo}}(T_1)-n_{\text{expt}}(T_1),d_s]$$
$$=\text{root}[n_{\text{theo}}(20.0)10^{-13}-3.97,d_s], \quad \text{(A2)}$$

$$N_{A,b}=\text{root}[\mu_{H,\text{theo}}(T_2)-\mu_{H,\text{expt}}(T_2),N_{A,b}]$$
$$=\text{root}[\mu_{H,\text{theo}}(100.1)-411,N_{A,b}], \quad \text{(A3)}$$

$$N_{D,b}=\text{root}[n_{\text{theo}}(T_3)-n_{\text{expt}}(T_3),N_{D,b}]$$
$$=\text{root}[n_{\text{theo}}(233.7)10^{-14}-1.40,N_{D,b}], \quad \text{(A4)}$$

$$E_{D,b} = \text{root}[n_{\text{theo}}(T_2) - n_{\text{expt}}(T_2), E_{D,b}]$$
$$= \text{root}[n_{\text{theo}}(100.1)10^{-13} - 1.96, E_{D,b}], \quad \text{(A5)}$$

and

$$R_{sc} = \text{root}[\mu_{H,\text{theo}}(T_3) - \mu_{H,\text{expt}}(T_3), R_{sc}]$$
$$= \text{root}[\mu_{H,\text{theo}}(233.7) - 273, R_{sc}]. \quad \text{(A6)}$$

Here, as examples, we have included the equations used to find set_1 for sample TD-3212–8d. For this sample, the three experimental temperature points chosen were $T_1 = 20.0$, $T_2 = 100.1$, and $T_3 = 233.7$ K. Note that, in this case, the high-temperature point was chosen to avoid data above 235 K since excitation from a deeper donor clearly becomes important above this temperature, and the theoretical model presented here is limited to a single donor. Indeed, multiple donors can easily be accommodated by replacing Eq. (7) with an appropriate transcendental equation[14] but such a complication is not warranted here since we are primarily interested in the surface conduction.

A MathCad file that performs the calculations based on Eqs. (3)–(19) and (A1)–(A6) for an arbitrary number of iterations is available by electronic mail from the author.[19]

[1]D. C. Look, Mater. Sci. Eng., B **80**, 383 (2001).
[2]S. J. Pearton, D. P. Norton, K. Ip, Y. W. Heo, and T. Steiner, Prog. Mater. Sci. **50**, 293 (2005).
[3]U. Ozgur, Y. I. Alivov, C. Liu, A. Teke, M. A. Reshchikov, S. Dogan, V. Avrutin, S. J. Cho, and H. Morkoc, J. Appl. Phys. **98**, 041301 (2005).
[4]L. Liao, H. B. Lu, M. Shuai, J. C. Li, Y. L. Liu, C. Liu, Z. X. Shen, and T. Yu, Nanotechnology **19**, 175501 (2008).
[5]O. Schmidt, P. Kiesel, C. G. Van de Walle, N. M. Johnson, J. Nause, and G. H. Döhler, Jpn. J. Appl. Phys., Part 1 **44**, 7271 (2005).
[6]D. C. Look, H. L. Mosbacker, Y. M. Strzhemechny, and L. J. Brillson, Superlattices Microstruct. **38**, 406 (2005).
[7]I. V. Markevich, V. I. Kushnirenko, L. V. Borkovska, and B. M. Bulakh, Solid State Commun. **136**, 475 (2005).
[8]G. H. Kassier, M. Hayes, F. D. Auret, M. Mamor, and K. Bouziane, J. Appl. Phys. **102**, 014903 (2007).
[9]O. Schmidt, P. Kiesel, D. Ehrentraut, T. Fukuda, and N. M. Johnson, Appl. Phys. A: Mater. Sci. Process. **88**, 71 (2007).
[10]D. C. Look, Surf. Sci. **601**, 5315 (2007).
[11]I. V. Tudose, P. Horváth, M. Suchea, S. Christoulakis, T. Kitsopoulos, and G. Kiriakidis, Appl. Phys. A: Mater. Sci. Process. **89**, 57 (2007).
[12]D. C. Look, B. Claflin, and H. E. Smith, Appl. Phys. Lett. **92**, 122108 (2008).
[13]R. L. Petritz, Phys. Rev. **110**, 1254 (1958).
[14]D. C. Look, *Electrical Characterization of GaAs Materials and Devices* (Wiley, New York, 1989).
[15]D. L. Rode, Semicond. Semimetals **10**, 1 (1975).
[16]B. R. Nag, *Electron Transport in Compound Semiconductors* (Springer-Verlag, Berlin, 1980).
[17]D. C. Look and J. R. Sizelove, Phys. Rev. Lett. **82**, 1237 (1999).
[18]MathSoft Inc., 101 Main Street, Cambridge, MA 02142.
[19]Program MOBCONCFIT in MATHCAD Version 13, available without cost from author at david.look@wright.edu
[20]Cermet, Inc., 1019 Collier Road, Suite C-1, Atlanta, GA 30318.
[21]Tokyo Denpa Co., Ltd., 5-6-11 Chuo, Ohta-ku, Tokyo 143-0024, Japan.
[22]D. C. Look, Superlattices Microstruct. **42**, 284 (2007).